Multi grain-size total sediment load model based on the disequilibrium length

Marine Le Minor, Philippe Davy, Jamie Howarth, Dimitri Lague

Multi grain-size total sediment load model based on the disequilibrium length

Marine Le Minor[1], Philippe Davy[1], Jamie Howarth[2], Dimitri Lague[1]

[1]University of Rennes 1, CNRS, Géosciences Rennes, UMR6118, Rennes, France

[2]School of Geography, Environment and Earth Sciences, Victoria University of Wellington, Wellington, New Zealand

Key Points:

- Emergence of a continuous description of sediment transport using the transport length model and the erosion-deposition framework
- Unified theory of sediment transport encompassing the diversity of transport modes such as bed load and suspended load
- Model applicable to both non-stationary and stationary regimes while showing that transport in suspension is likely never at capacity

Corresponding author: Marine Le Minor, marine.le-minor@univ-rennes1.fr

This article has been accepted for publication and undergone full peer review but has not been through the copyediting, typesetting, pagination and proofreading process, which may lead to differences between this version and the Version of Record. Please cite this article as doi: 10.1029/2021JF006546.

Abstract

In natural rivers, sediment heterogeneity and flow variability control the diversity of transport modes that occur. Although these different modes contribute to the total sediment transport, a law extending from bed load to suspended load that is relevant for a wide range of sediment mixtures and flow conditions is lacking. Besides, a transport-limited assumption is often made in modeling of fluvial morphodynamics and thus potentially misses under-/over-capacity regimes associated with a particular range of grain sizes and hydraulic conditions. We present a Multi Grain-Size Total Load model based on widely accepted concepts of sediment transport and developed within the transport length framework in combination with an erosion-deposition formulation. The new transport length model captures the diversity of transport modes as a physical continuum. Transport capacities for single or bimodal grain sizes are reasonably predicted when compared to published data and scale with the bed shear stress through a continuously varying exponent linked to the characteristic transport height. Modeled transport lengths extend over several orders of magnitude at given flow conditions. Extremely long distances suggest that suspended transport is probably never at capacity. The model can be extended to populations of various grain sizes with a threshold of motion corrected from hiding-exposure. However, further experimental constraints are needed to better describe entrainment and saltation in strongly heterogeneous bed load transport. The new theoretical formalism we introduce paves the way for a Multi Grain-Size Total Load Sediment Transport model that includes the variety of transport modes in both non-stationary and stationary regimes.

Plain Language Summary

In natural rivers, flow variability and sediment heterogeneity affect how sediment grains are transported. Whether grains move close to the bed or higher in the water column, they all contribute to the total sediment transport as bed load and suspended load, respectively. However, a unique law that predicts the total amount of sediment that can be transported by a river for a wide range of sediment mixtures and flow conditions is lacking. Besides, in modeling of fluvial morphodynamics, the river is often assumed at capacity, meaning that it carries the maximum sediment load it can, and thus under-/over-capacity regimes are potentially missed. We present a Multi Grain-Size Total Load model, built by bringing together widely accepted concepts of sediment transport, that includes the variety of transport modes in both capacity and under-/over-capacity regimes. The two main components of this

model are: 1) the transport length defined as the distance over which sediments are transported and, 2) the erosion-deposition formulation that explicitly describes the transfer of sediment from the sediment bed to the above water column, and conversely. While the new transport length model captures the transport from bed load to suspension continuously, the erosion-deposition model applies to several grain sizes.

1 Introduction

In a river, the erosion of sediment grains and their transport are two processes at stake. To account for these processes in modeling river morphodynamics, two approaches exist: i) an equilibrium between hydraulic conditions and capacities is assumed and the topographic changes are calculated as a spatial gradient of capacities, ii) exchanges between the water column and the sediment bed are described with the deposition and erosion rates. This second approach is made possible by using the erosion-deposition framework (Krone, 1962; Partheniades, 1965; Hairsine & Rose, 1992), where erosion and deposition can be linked by a transport length that depends on the grain ejection height, the hydraulic conditions and the sediment properties. This length is defined as the distance required by the sediment transport rates to adjust to a disturbance, i.e., when erosion and deposition balance each other again after a change in bed shear stress (Daubert & Lebreton, 1967; Jain, 1992; Kooi & Beaumont, 1994; Charru, 2006; El kadi Abderrezzak & Paquier, 2009). Thus, this transport length is a lag distance also refered to as a disequilibrium length. It is important for simulating transient states (Fernandez-Luque & Beek, 1976; Galappatti & Vreugdenhil, 1985; Davy & Lague, 2009) and to study unsteady morphodynamic systems such as bed forms (Ganti et al., 2014) and braiding patterns (Davy & Lague, 2009).

Through their motion, individual sediment grains contribute to the overall sediment transport. Under the same flow conditions, sediment grains of varying sizes are transported differently resulting in different transport modes defined according to the frequency of contact with the bed. The mode of transport depends on the transport stage $T^* = \tau/\tau_c - 1$ where τ [Pa] is the bed shear stress and τ_c [Pa] is the critical bed shear stress of the sediment (Yalin, 1972; Ackers & White, 1973; van Rijn, 1984a). A positive transport stage means that grains are in motion. In the vicinity of the threshold of motion, bed load transport dominates and sediment grains are in frequent contact with the bed. They roll at very low transport stages $T^* < 1$ and move through intermittent jumps, meaning they alternate periods of rest and saltation, at low to moderate transport stages $1 < T^* < 100$ (Auel

et al., 2017). For $T^* > 100$, suspension dominates and sediment grains are transported over the water column instead of concentrating in a layer near the bed. Depending on the flow intensity, the same grain may be resting, transported as bed load or suspended load (Hjulström, 1935). Water discharge events are key drivers of landscape evolution since very large, infrequent floods may cause suspension of grains that are most of the time transported as bed load (Larsen & Lamb, 2016). Therefore, it is important to incorporate changes in motion regime of sediment grains from bed load to suspended load when water discharge variability is considered. Similarly, the knowledge of the partitioning of total sediment load into bed load and suspended load remains difficult to define (Turowski et al., 2010) as are transport capacities (often called "transport laws") for a wide range of grains sizes due to concomitant bed load and suspended load transport.

To our knowledge, there is no framework based on the disequilibrium length, which integrates a whole grain size distribution and that connects saltation with suspension. To account for the different modes of transport in modeling morphodynamic instabilities, one attempt has been made to produce a continuous model of particle transport length that covers two modes of transport, namely saltation and suspension (Naqshband et al., 2017). Naqshband et al. (2017) suggest to use two equations that differs in form: one for the transport in saltation and one for the suspension. In this paper, we propose a conceptual advance of the disequilibrium length framework to account for both bedload and suspended load. Our approach could be used to study river systems that are not at equilibrium, i.e., either at over- or under-capacity. The concept of under- and over-capacity emerges from the ratio between the deposition rate and the erosion rate, two fluxes that have different domains of variations. Under-capacity corresponds to the erosion rate that prevails over the deposition rate after, for instance, a slope increase. By symmetry, over-capacity corresponds to the deposition rate that prevails over the erosion rate. These transient responses occur over a finite distance whose extent depends on the disequilibrium length. The distance will be very short for bed load and longer for suspended load.

Most of the transport laws consider bed load only (e.g., Meyer-Peter & Müller, 1948) or suspended load only (van Rijn, 1984b). Total load may be described as a whole (Engelund & Hansen, 1967) or as a sum of the bed load and suspended load contributions (van Rijn, 1984b). Transport laws were established by correlating measurements of the shear stress exerted on the sediment bed and the sediment transport rate per unit flume width at equilibrium, also referred to as stream capacity.

Transport laws that account for sediment heterogeneity in size consider the transport of each grain size through its fraction in a sediment mixture and by considering grain interactions through a corrected threshold of motion (Kleinhans & van Rijn, 2002; Wilcock & Crowe, 2003). The threshold of motion of heterogeneous sediments differs from that of monodisperse sediments due to hiding-exposure effects (Einstein, 1950; Wilcock, 1993). While fine grains are harder to put in motion when they are sheltered behind coarse grains, coarse grains are easier to entrain when they stick out of surrounding fine grains. The threshold of motion is a key parameter in the erosion of sediment grains since it gives the value of shear stress that needs to be exceeded for grains to be ejected from the sediment bed to the water column.

Despite the large number of grain-scale and reach-scale studies on sediment transport (e.g., Meyer-Peter & Müller, 1948; Engelund & Hansen, 1967; van Rijn, 1984a, 1984b; Charru et al., 2004; Lajeunesse et al., 2010; Houssais & Lajeunesse, 2012), there is no continuous transport law that covers both bed load and suspended load for a wide range of flow strengths and grain sizes. Such a unified theory of sediment transport should ideally capture both the different modes of transport and the magnitude and scaling of transport rates, but also potential grain interactions due to sediment heterogeneity. Meeting these requirements is a challenge since the continuous model of sediment transport must rely on widely accepted notions and predict well justified equations or experiments. Using the erosion-deposition formulation in combination with the transport length framework linking saltation to suspension could help to fill this gap since a simple relationship emerges at equilibrium: the stream capacity is equal to the product of the transport length and the erosion rate (Davy & Lague, 2009). In addition, grain-scale studies have contributed to the parametrization of the erosion-deposition formulation through the measurement of fluxes at equilibrium: first derived from viscous flow studies (Charru et al., 2004), it has been extended later to turbulent flows and both uniform and bimodal sediments (Lajeunesse et al., 2010; Houssais & Lajeunesse, 2012).

In this paper, we aim to gather concepts and observations on sediment transport in order to: 1) build a continuous formulation of transport length that covers the variety of sediment transport processes ; 2) develop by extension a continuous model of sediment transport from bed load to suspended load for a population of grain sizes. The self-consistent theory presented in this paper remains as simple (reduced complexity) as possible while keeping its physical relevance through the use of few parameters that represent basic physical processes.

The parameterization of Davy and Lague (2009) for the transport length serves as a base to our continuous model of transport length, as well as the work by Einstein (1950) and Wilcock (1993) for the effect of surface grain size heterogeneity on entrainment threshold. The originality of our work resides in the consideration of a characteristic transport height parameter that describes the transport mode spectrum as a continuum. Then, the continuous formulation of transport length is put to use for the calculation of sediment transport rates. To illustrate the performance of our continuous model of sediment transport, basic model predictions for bed load, suspended load and total load are compared to experimental data. Sensitivity analyses are carried out to identify the most influencing parameters. Ultimately, we show that our continuous transport length model has the power to predict stream capacities for a wide range of grains sizes that are rolling, saltating or in suspension while accounting for sediment heterogeneity. However, limits in our understanding of saltating dynamics in strongly heterogeneous sediment transport hamper our ability to offer a fully calibrated universal sediment transport model.

2 Erosion-deposition model

In this paper, we extend the model of Davy and Lague (2009), based on a single-grain approach, to several grain sizes. To do so, we introduce grain size-specific parameters and we adapt the equations of the transport length model and of the erosion-deposition framework to account for a spectrum of grain sizes. The model is fully defined by the two expressions of the fluxes, erosion $\dot{e}$ and deposition $\dot{d}$, or by the erosion rate $\dot{e}$ and the transport length ξ. This transport length ξ depends on the ejection height h_s, the settling velocity w_s and the horizontal velocity of particles $\overline{v}_s$ so that the model comes to define four main parameters (Figure 1):

- the erosion rate $\dot{e}$;
- the particle ejection height h_s;
- the particle settling velocity w_s;
- and the particle horizontal velocity $\overline{v}_s$.

2.1 Mass balance equations

Two systems are considered: the flowing water column that contains mobile sediments and the sediment bed that is a layer of immobile sediments at the base of the flow. Sediment

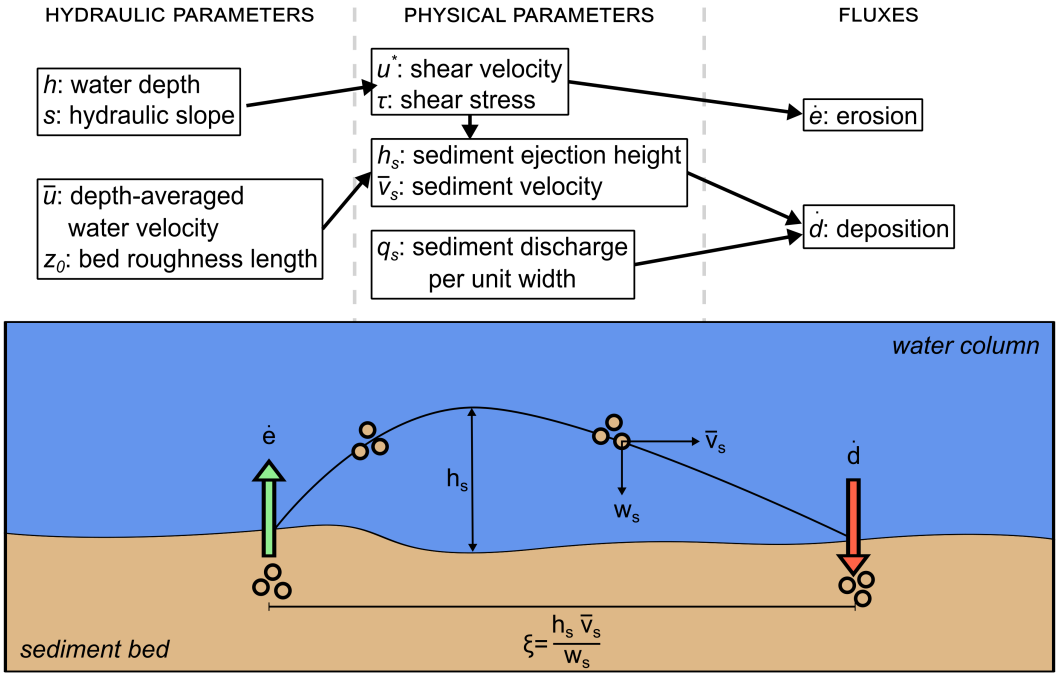

Figure 1. Sketch showing the model parameters and the role they play in the transport length that links erosion and deposition.

transport results from the exchanges that occur between these two systems. Erosion is the physical process that corresponds to the transfer of sediment from the sediment layer to the stream; conversely, deposition encompasses the transfer that goes the other way around. In the erosion-deposition framework, the erosion and deposition rates are explicit physical processes and not included in a single term such as the divergence of the sediment load. For the transported sediment in the water column, the mass balance equation is defined in the Eulerian frame as:

$$\frac{\partial (C_s\, h)}{\partial t} + div\,(q_s) = \dot{e} - \dot{d} \tag{1}$$

where C_s [-] is the depth-averaged sediment concentration, $\dot{d}$ [m·s^{-1}] is the deposition rate, $\dot{e}$ [m·s^{-1}] is the erosion rate, h [m] is the water depth and q_s [m^2·s^{-1}] is the sediment load per unit width.

The sediment load per unit width q_s is related to the stream discharge per unit width q [m^2·s^{-1}] as follows:

$$q_s = C_s\, q = C_s\, u\, h \tag{2}$$

where u [m·s^{-1}] is the average flow velocity.

2.2 Erosion rate

The basal shear stress exerted by the flow on the sediment bed depends on the water discharge q and the topographic slope. Following studies measuring grain scale dynamics and macroscopic sediment fluxes (Charru et al., 2004; Lajeunesse et al., 2010), we assume that the erosion rate $\dot{e}$, also referred to as the entrainment rate, increases linearly with the excess of bed shear stress as (Partheniades, 1965):

$$\dot{e} = k_e\ (\tau - \tau_c) \tag{3}$$

where k_e [m^2·s·kg^{-1}] is the entrainment coefficient that incorporates the effect of sediment properties (e.g., grain size).

Lajeunesse et al. (2010) proposes a formulation of the entrainment coefficient that appears to hold for bimodal mixtures (Houssais & Lajeunesse, 2012). We thus assume that their formulation holds for any sediment mixtures and the erosion coefficient is expressed as (Lajeunesse et al., 2010):

$$k_e = \frac{\pi}{6}\,\frac{c_e}{\rho_s\, w_s} \tag{4}$$

where c_e [-] is an empirical constant, ρ_s [kg·m^{-3}] is the sediment density and w_s [m·s^{-1}] is the sediment fall velocity. This entrainment coefficient is proportional to the inverse of the settling velocity as was previously reported in the literature (Garcia & Parker, 1991). The value of c_e is calibrated from measurements of saturated density of bed load grains in the flume experiment of Lajeunesse et al. (2010). We assume that this coefficient is independent of grain size and also valid for suspended load. The definition of the entrainment coefficient k_e that controls the erosion rate $\dot{e}$ and its generalization to any grain size is a new development of the erosion efficiency factor mentioned in Davy and Lague (2009).

For fine grains ($d < 100$ µm), the settling velocity is equivalent to the Stokes' law: $w_s = R\, g\, d^2/18\, \nu$ where d [m] is the sediment grain diameter, g [m·s^{-2}] is the gravity, $R = \rho_s - \rho/\rho$ [-] is the sediment specific gravity (ρ [kg·m^{-3}] is the water density) and

ν [$m^2 \cdot s^{-1}$] is the kinematic viscosity of water. For coarse grains ($d > 1$ mm), the settling velocity becomes $w_s \propto \sqrt{R\,g\,d}$, which is equivalent to the Newton's law. In this paper, we choose to calculate the settling velocity w_s with the formula of Ferguson and Church (2004) that captures the fall velocity of sediment grains in water over a wide range of sizes and hydrodynamic conditions (viscous to turbulent). It explicitly encompasses the two known asymptotic trends on both sides of the particle size spectrum.

Here are a few remarks regarding the erosion rate formulation: 1) The erosion rate depends on the sediment grain properties (diameter, density, settling velocity and threshold of motion); 2) The threshold of motion is explicit with no erosion unless the critical shear stress is exceeded; 3) The various trends of the fall velocity lead to different regimes of erosion rate. The entrainment coefficient k_e scales with $c_e\,d^{-2}$ for fine grains ($d < 100$ µm), while it scales with $c_e\,d^{-0.5}$ for coarse grains ($d > 1$ mm). The variations of the entrainment coefficient k_e are consistent with the fact that coarse grains are subject to longer periods of rest than fine grains that spend more time without any contact with the bed (Liu et al., 2019).

Computation steps of the erosion rate are provided in Appendix A.

2.3 Deposition rate

In the perspective of a unified theory, we consider that sediment is mostly transported in a layer extending from the top of the alluvial cover with a thickness h_s [m] smaller or equal to the water depth h. This means that the sediment load in this transport layer of thickness h_s is approximately the sediment load q_s of the stream.

The number of grains that fall from the stream onto the bed define the deposition rate $\dot{d}$ (Krone, 1962):

$$\dot{d} = C_s^*\, w_s \tag{5}$$

where C_s^* [-] is the sediment concentration in the portion of the water column where most of the sediment transport occurs.

Considering a population of grains with similar properties (e.g., size), we make the assumption that all the grains within the layer of dominant transport travel at the same average velocity $\overline{v}_s$ [$m \cdot s^{-1}$]. The sediment concentration in this layer may thus be described

as the ratio of the sediment flux over the whole water depth to the sediment flux in the layer where most transport takes place:

$$C_s^* = \frac{q_s}{h_s\,\overline{v}_s} \tag{6}$$

The deposition rate $\dot{d}$ may, therefore, be written as:

$$\dot{d} = \frac{q_s}{h_s\,\overline{v}_s} w_s \tag{7}$$

We make the hypothesis that the deposition rate may write as $\dot{d} = q_s/\xi$, where ξ [m] is the transport length for a given grain size. This formalism was introduced by Kooi and Beaumont (1994). Ultimately, the transport length ξ is as follows:

$$\xi = \frac{h_s\,\overline{v}_s}{w_s} \tag{8}$$

This formulation of the transport length ξ is similar to the one of Davy and Lague (2009).

Computation steps of the deposition rate are provided in Appendix A.

2.4 Parametrization of the disequilibrium length

2.4.1 Characteristic height h_s

The newness of our work with respect to the transport length model presented by Davy and Lague (2009) mainly resides in the definition of a key parameter: the characteristic transport height h_s, which can be seen as an average grain ejection height. Whereas Davy and Lague (2009) employed two different definitions, one for bed load and one for suspended load, we present a transport length model that relies on a single expression of the characteristic transport height h_s encompassing a continuum of transport modes, namely, saltation and suspension.

Experimental studies on saltation height showed that the saltation height h_{salt} [m] increases with T^* (see Ali and Dey (2019) for a review). However, there is no consensus on how the saltation height h_{salt} scales with the transport stage T^*, likely due to the variety of hydraulic conditions and sediment properties studied. When saltation dominates, we suppose that the characteristic transport height h_s can be written as:

$$h_{salt} = \alpha\, d \;+\; a\, d\, T^{*b} \tag{9}$$

where $\alpha = 0.6$, a=0.025 and b=1 are two constants whose value comes from published empirical formulas of grain saltation height (Auel et al., 2017).

To connect saltation with suspension, we make the hypothesis that the characteristic transport height h_s [m] may be expressed as a sigmoidal function (Figure 2a) bounded by the saltation height h_{salt} and the water depth h:

$$h_s = h_{salt} + \frac{h - h_{salt}}{r_0} \tag{10}$$

where r_0 [-] is the gradient of vertical sediment distribution used to calculate the suspension height h_s when suspension occurs. According to Equation 10, this gradient may be described as a ratio of heights $r_0 = (h - h_{salt}) \,/\, (h_s - h_{salt})$ and is used to determine how the thickness of the layer of dominant transport exceeds the saltation height. For very large values of r_0, the portion of the water column where most sediment transport takes place is constricted within the saltation layer and bed load is the dominant transport process. For a r_0 of 1, sediment transport mostly occurs in suspension and extends uniformly over the whole water column.

A common parameter to assess the dominant mode of sediment transport is the Rouse number P [-]. Its value describes the shape of the concentration profile between a reference height z_{ref} [m] taken as the bed roughness length z_0 [m] and the water depth. Assuming a logarithmic velocity profile, the sediment concentration profile of Rouse (1937) is described by the following equation:

$$C_s = C_{s,ref} \left(\frac{h - z}{z} \frac{z_{ref}}{h - z_{ref}} \right)^P \tag{11}$$

where $C_{s,ref}$ [-] is the sediment concentration at the reference height.

Field and laboratory observations have shown that the ratio of the sediment diffusivity to the eddy viscosity plays a role in the distribution of the suspended sediment through the water column (van Rijn, 1984b; Rose & Thorne, 2001; Camenen & Larson, 2008; Santini et al., 2019; de Leeuw et al., 2020). Thus, the Rouse number may be modulated by a diffusivity ratio β [-] that represents the behaviour of sediment grains with respect to the flow (Graf & Cellino, 2002):

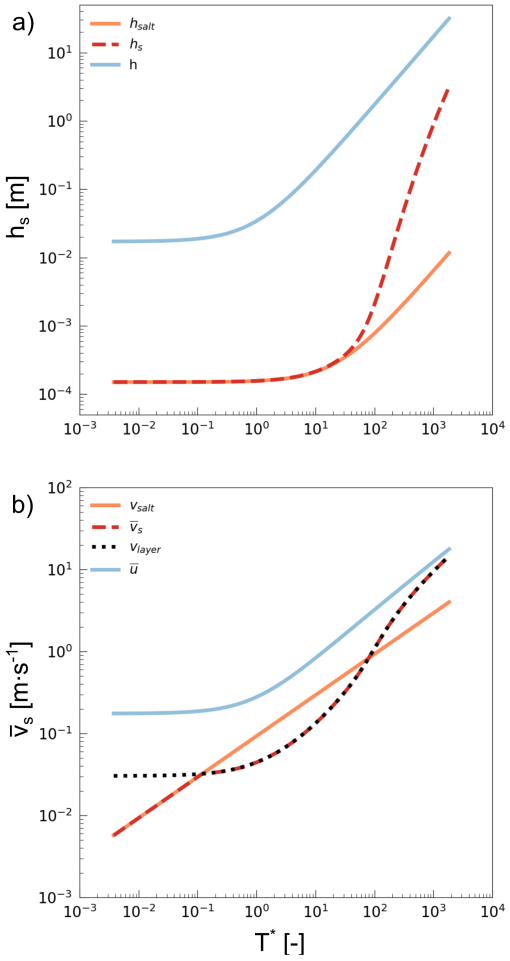

Figure 2. Characteristic transport parameters. a) Characteristic transport height h_s (Equation 10) and characteristic transport velocity $\overline{v}_s$ (Equation 16) plotted against the transport stage T^* for a grain size of 250 µm, a slope of 0.001 and a water depth ranging from 1 cm to 30 m. The bed shear stress was calculated as $\tau = \rho\, g\, h\, s$ and a bed roughness of $z_0 = 3\, d/30$ was assumed. $\overline{u}$ corresponds to the average flow speed over the whole water depth (assuming a logarithmic profile), v_{layer} to the average flow speed over the characteristic height of transport (Equation 15) and v_{salt} to the saltation velocity (Equation 14).

$$P = \frac{w_s}{\beta\,\kappa\,u^*} \tag{12}$$

where κ [-] is the von Kármán constant (κ=0.41) and u^* [m·s^{-1}] is the shear velocity. The ratio of sediment diffusivity to eddy viscosity β is commonly assumed equal to 1, meaning that sediment grains move at the velocity of the water that carries them (Rouse, 1937). For further calculations in this paper, we take $\beta = 1$.

To calculate the gradient of sediment distribution r_0, we first assume that when suspension occurs, h_{salt} is very small compared to both the water depth h and the suspension height h_s such that $r_0 \approx h/h_s$. Then we assume that the gradient r_0 corresponds to the ratio between the mean sediment concentration in the entire water column and the sediment concentration at the reference height $z_{ref} = z_0$. It is defined as:

$$r_0 = \frac{C_{s,ref}}{C_s} = C_{s,ref}\,\frac{q}{q_s} = C_{s,ref}\,\frac{\int_{z_0}^{h} u\,(z)\,h\,dz}{\int_{z_0}^{h} C_s\,(z)\,u\,(z)\,h\,dz} = \frac{\int_{z_0}^{h} ln\left(\frac{z}{z_0}\right) dz}{\int_{z_0}^{h} \left(\frac{h-z}{z}\frac{z_0}{h-z_0}\right)^{P} ln\left(\frac{z}{z_0}\right) dz} \tag{13}$$

where u [m·s^{-1}] is the water velocity assumed to follow a vertical logarithmic profile. Note that knowing the reference contration $C_{s,ref}$ is not needed since its cancels itself in Equation 13.

A similar approach to encompass the complexity of the concentration profile in a single parameter has been presented in Davy and Lague (2009) with an attempt to calculate the disequilibrium length of suspended sediment. We used sums to approximate the integrals and to obtain values of distribution gradient r_0.

2.4.2 Characteristic velocity $\overline{v}_s$

The characteristic transport velocity $\overline{v}_s$ represents the average travel velocity of sediment grains in the flow from entrainment to re-deposition.

Saltating grains tend to move more slowly than the surrounding water (Fernandez-Luque & Beek, 1976). The velocity of grains in saltation v_{salt} [m·s^{-1}] may be expressed as (Auel et al., 2017):

$$v_{salt} = 1.46\,\sqrt{R\,g\,d}\,T^{*0.5} \tag{14}$$

We assume that saltation velocities calculated with Equation 14 can not exceed the average water velocity v_{layer} [m·s^{-1}] over the characteristic transport height h_s that stems from the integration of the log-law velocity profile between the bed roughness z_0 and the characteristic height h_s:

$$v_{layer} = \frac{1}{h_s} \int_{z_0}^{h_s} \frac{u^*}{\kappa} \ln\left(\frac{z}{z_0}\right) dz = \frac{u^*}{\kappa} \left(\ln\left(\frac{h_s}{z_0}\right) - 1 + \frac{z_0}{h_s}\right) \tag{15}$$

The characteristic sediment transport velocity $\overline{v}_s$ of transported grains thus writes:

$$\overline{v}_s = \begin{cases} \min\left(v_{salt}, v_{layer}\right), & \text{if } P \geq 2.5 \\ v_{layer}, & \text{if } P < 2.5 \end{cases} \tag{16}$$

Figure 2b illustrates these two regimes of sediment velocity. In this example, the characteristic transport velocity $\overline{v}_s$ is equivalent to the saltation velocity v_{salt} at transport stage values below 10^{-1}, while it is similar to the averaged water velocity in the layer of transport v_{layer} above.

2.5 Transport capacity laws

At equilibrium, when the sediment load in the stream varies neither spatially nor temporarily, deposition and erosion balance each other ($\dot{e} = \dot{d}$) and, as a consequence, the sediment load in the river system is equivalent to the stream capacity q_s^{eq} [m^2·s^{-1}]. Replacing the transport length ξ and the erosion coefficient k_e in the relationship between erosion rate $\dot{e}$ and stream capacity q_s^{eq} by their expressions (Equations 4 and 8), the equilibrium sediment load can be written as:

$$q_s^{eq} = \xi\, \dot{e} = \xi\, k_e\, (\tau - \tau_c) = \frac{\pi}{6}\, c_e\, \frac{h_s\, \overline{v}_s}{\rho_s\, {w_s}^2}\, (\tau - \tau_c) \tag{17}$$

Transport laws are commonly expressed in dimensionless form using the Shields number θ [-] in place of the shear stress τ. The Shields number (Shields, 1936) is defined as:

$$\theta = \frac{\tau}{\rho\, R\, g\, d} \tag{18}$$

For the same purpose, the dimensionless transport rate, or Einstein number (Einstein, 1950), q_s^* [-] is defined as:

$$q_s^* = \frac{q_s}{\sqrt{R\,g\,d^3}} \tag{19}$$

Consequently, the dimensionless transport rate at equilibrium derived from our model is expressed as:

$$q_s^{eq*} = \frac{\pi}{6}\,c_e\,\frac{\rho}{\rho_s}\,\frac{h_s}{d}\,\frac{\sqrt{R\,g\,d}\,\overline{v}_s}{{w_s}^2}\,(\theta - \theta_c) \tag{20}$$

Equation 20 is an equilibrium model for the total load of a given grain size. It includes a critical threshold as in many transport laws, especially for bed load. Indeed, we will show below that our model is similar in form to Meyer-Peter and Müller (1948), Kleinhans and van Rijn (2002), Lajeunesse et al. (2010), among others. The scaling behaviour of the transport capacity q_s^{eq} with the bed shear stress τ depends on the characteristic height h_s and velocity $\overline{v}_s$. The scaling value m [-] such as $q_s^{eq*} \propto (\theta - \theta_c)^m$ will be investigated later.

In the following we assume that the model introduced in this section is applicable to sediment mixtures by accounting for the fraction of the *ith* size in the erosion and deposition equations, and by modifying the critical threshold to account for the collective effect of multiple grain size.

Computation steps of the sediment transport capacity are provided in Appendix A.

3 Elements of calibration

The only model parameter that requires calibration is the erosion constant c_e and we estimated it using the data presented in Lajeunesse et al. (2010) for single grains and Houssais and Lajeunesse (2012) for bimodal mixtures. Bedload transport was studied by measuring fluxes of spherical sediment grains. In their erosion-deposition model, the erosion rate $\dot{n_e}$ [$\mathrm{m^{-2}{\cdot}s^{-1}}$] is:

$$\dot{n_e} = \frac{F}{d^2\,t_e} \tag{21}$$

where F [-] is the sediment fraction, t_e [s] is the erosion time defined as $t_e = \rho_s d w_s / c_e\,(\tau - \tau_c)$.

The deposition rate $\dot{n_d}$ [$\mathrm{m^{-2}{\cdot}s^{-1}}$] is defined as:

$$\dot{n_d} = \frac{n}{t_d} \tag{22}$$

where n [m^{-2}] is the surface density of moving grains and t_d [s] is the deposition time.

Similar to Lajeunesse et al. (2010) and Houssais and Lajeunesse (2012), we consider a deposition time that depends on the grain size. Knowing that no suspension occured in their experiments, we assume that the deposition time should encompass the duration of the saltation jump, i.e., $t_d \propto h_{salt}$. The saltation height depends on the shear stress (Equation 9); however, the dependence of the deposition time on the shear stress was not accounted for by Lajeunesse et al. (2010) and Houssais and Lajeunesse (2012). In this paper, we define a grain-size and shear-stress dependent deposition time:

$$t_d = \frac{h_s}{w_s} \approx \frac{h_{salt}}{w_s} \tag{23}$$

Assuming a steady and spatially uniform flow, we have $\dot{n_d} = \dot{n_e}$. Thus, the number of moving particle at saturation n_{sat} [m^{-2}] writes as:

$$\frac{n_{sat}\, d^2}{F} = \frac{t_d}{t_e} = c_e\, \frac{\rho}{\rho_s}\, \frac{R\, g\, d}{{w_s}^2}\, \theta_c\, \left(\alpha\, T^* + a\, {T^*}^{1+b}\right) \tag{24}$$

Critical Shields values estimated by Lajeunesse et al. (2010) and Houssais and Lajeunesse (2012) were also used. Based on bed load data only, the linear regression on all the experimental data gives c_e=37.64 (R^2=0.71) (Figure 3a) and leads to an erosion coefficient k_e that varies over three orders of magnitude (Figure 3b).

4 Model consistency and validation

4.1 Transport length

The modeled transport lengths differ significantly from saltation lengths l_{salt} [m] and excursion lengths l_{susp} [m] reported in the literature (Figure 4). Indeed, our model predicts transport lengths that are at least one order of magnitude smaller than the saltation lengths (see Ali and Dey (2019) for a review) and at least three orders of magnitude smaller than the excursion lengths observed by Naqshband et al. (2017) under similar conditions tested in flume studies. These results suggest that predicted transport lengths are not comparable to

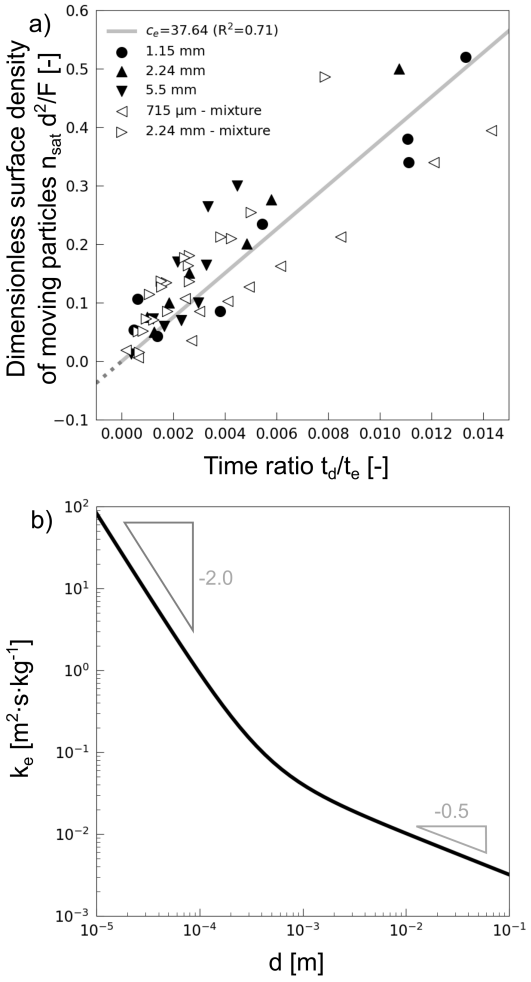

Figure 3. Model calibration. a) Linear regression of the erosion constant c_e based on data gathered by Lajeunesse et al. (2010) and Houssais & Lajeunesse (2012), b) Plot of k_e against grain diameter d.

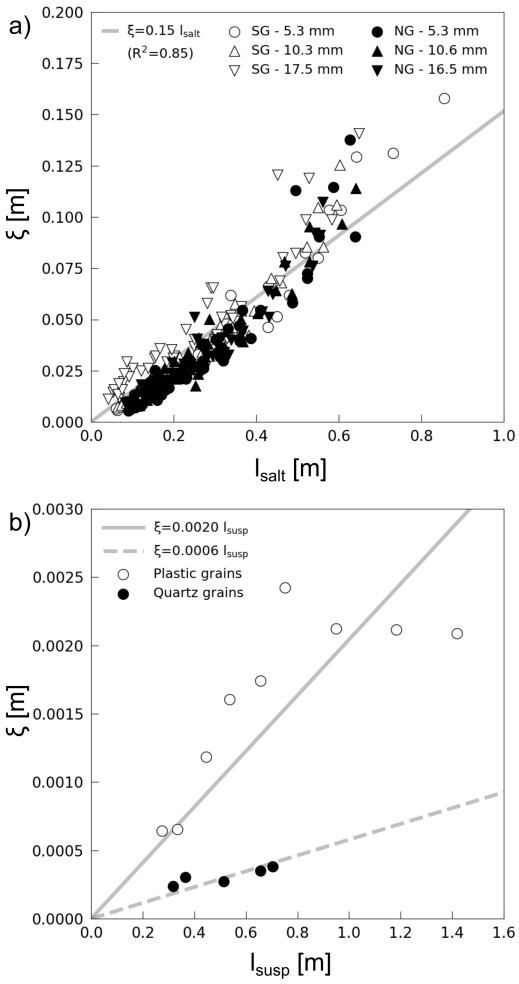

Figure 4. Comparison of modeled transport lengths with measured saltation and excursion lengths. Model predictions plotted a) against saltation lengths measured by Auel et al. (2017) for spherical grains (SG) and natural grains (NG) and, b) agains excursion lengths measured by Naqshband et al. (2017) for plastic and sediment grains of various sizes.

particle travel distances measured in the laboratory or in the field. The difference between our theory based on flux and experiments on single particles may explain this discrepancy.

Figure 5a inspired by the Hjulström diagram (Hjulström, 1935) shows that the characteristic height h_s formulation presented in this paper illustrates the different transport behaviors as well as the transition from one mode of transport to the other. Whereas the h_s/h ratio varies between 0 and 1 for fine sediment for a wide range of shear stress values, it increases from about 0 at low shear stress to less than 0.1 for high stress values for coarse grains. This shows that fine sediment grains, smaller than ∼0.1 mm are systematically

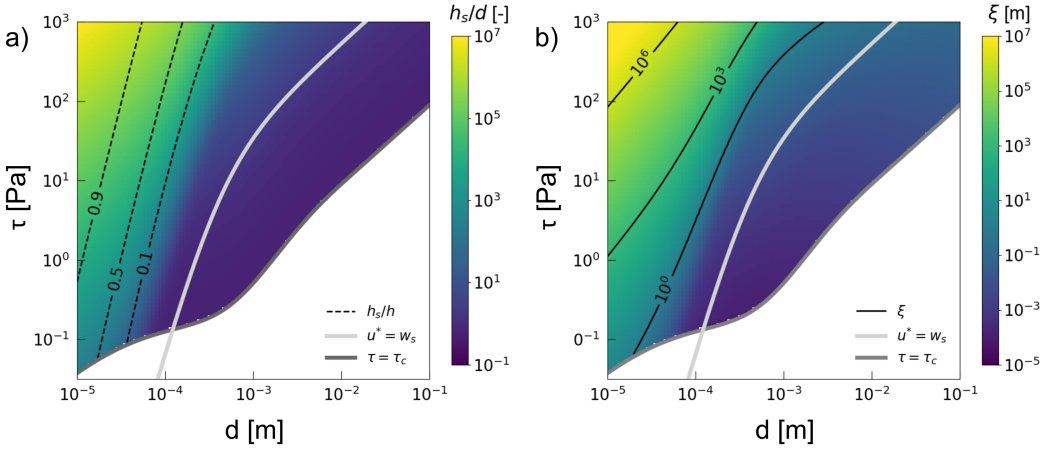

Figure 5. Characteristic height to grain diameter ratio h_s/d (a) and transport length ξ (b) for a bed roughness of $3\,d/30$, a slope of 0.001, water depths ranging from 1 cm to 30 m, shear stress values ranging from 10^{-2} to 10^3 Pa and sediment grain diameters varying from 10 µm to 10 cm. The Shields curve that gives the critical shear stress for initiation of motion is plotted in dark gray and the curve that corresponds to initiation of suspension $u^* = w_s$ is plotted in light gray.

transported in suspension over most of the water depth regardless of the bed shear stress, while coarse grains exhibit different transport height regimes: rolling, saltation and suspension but tend to remain concentrated at the bottom of the water column. This result is consistent with the familiar Hjulström diagram.

Figure 5b shows transport length values for a wide range of grain sizes assuming a slope of 0.001 and a bed shear stress varying with water depth. It appears that the transport lengths of grains coarser than 100 µm exhibit a slow increase with larger bed shear stress, whereas fine grains present a sharp rise in transport length values. Considering the shear stress range presented in Figure 5a, when the transport length of fine grains (d=50 µm) covers seven orders of magnitude and reaches 10^4 m, the transport length of coarse grains (d=5 cm) only varies over one and is up to 1 m (Figure 5b). These magnitudes suggest that coarse grains saturate over short distances, while fine grains need very long distances (up to $\sim 10^3$ km) to reach equilibrium and depending on the spatial scale considered may never be at saturation. The strong variations of transport length with grain size stresses the need to use a grain size-specific transport length. The characteristic height of transport may be smaller for finer grains than coarse ones since the finer grains tend to be transported in saltation or suspension at heights that are lower than the diameter of coarse grains.

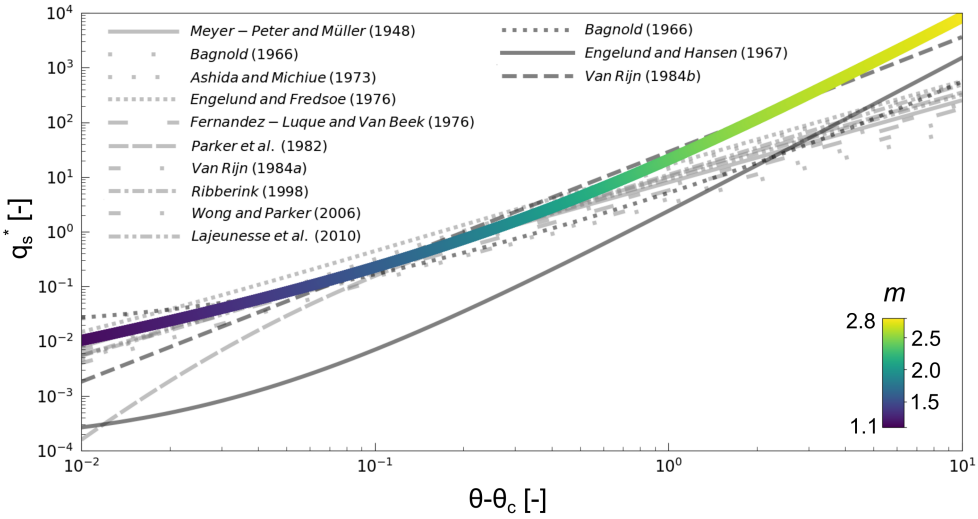

Figure 6. Comparison between model predictions and existing transport capacity laws. Example given for a grain size of d=1 mm, a slope of 0.005, a bed roughness $z_0 = 3d/30$, a Manning coefficient of 0.02 and a water depth h ranging from 1 cm to 30 m. Continuous values of scaling exponent m illustrate the connection between bedload and suspended load.

4.2 Comparison with published data of sediment load

Assessing the asymptotic behavior of the transport rates is one way to indirectly validate our model. Furthermore, the comparison of modeled saturated transport rates with experimental data allows for an evaluation of its predictive capabilities. Our Multi Grain-Size Total Load model considers a grain size-specific threshold of motion and, when it is exceeded, a non-zero sediment transport rate value is modeled. Thus, for the comparison with flume measurements, we only took into account the grain sizes that are predicted in motion by our model in spite of experimental data exhibiting non-zero and positive transport rates that contradict the predictions of no motion.

4.2.1 Bed load transport

First, we assess our model predictions for bed load transport considering a single grain size. Many published bed load transport formulas predict that the dimensionless transport rate at equilibrium scales with the excess Shields number as $q_s^{eq*} \propto (\theta - \theta_c)^{1.5}$ (Meyer-Peter & Müller, 1948; Bagnold, 1966; Ashida & Michiue, 1973; Engelund & Fredse, 1976; Fernandez-Luque & Beek, 1976; Parker et al., 1982; van Rijn, 1984a; Ribberink, 1998; Wong

& Parker, 2006; Lajeunesse et al., 2010). Modeled transport capacities fall within the range of magnitudes reported in literature. They exhibit a scaling m that spreads from 1.1 to 2.1 for $10^{-2} < \theta - \theta_c < 5 \times 10^{-1}$ and thus appears to vary around the value of 1.5 mentioned previously (Figure 6).

For further assessment of the performance of our model in terms of magnitude, we compare the values of transport capacities predicted by our model to flume measurements. To do so, values of bed load transport predicted by our model were compared to the ones measured by Lajeunesse et al. (2010) for similar hydraulic conditions and sediment properties. For the comparison with Lajeunesse et al. (2010), we used the critical threshold of motion (Table 3 in their paper) and the bed roughness length they measured. We assume that all grain sizes were at saturation since the transport lengths, up to 3 mm, are very short compared to the 2-m-long flume. Overall, the model appears to reasonably estimate transport capacities since 95% and 100% of the experimental data are predicted within a factor of 5 and 10, respectively (Figure 7a). Factors of 5 and 10 are believed to be sufficient for a first attempt at developing a completely new theory on multi grain-size total load transport (i.e., potentially unlimited number of grain sizes) under various hydraulic conditions. The good results may be explained by the fact that we calibrated our model through the erosion coefficient k_e against their flume data. Furthermore, the data used by Meyer-Peter and Müller (1948) were extracted from the ETH report by Smart and Jaeggi (1983). Parameters such as water depth, water discharge, flume width, sediment grain size, sediment load serve as inputs for our calculations. The critical Shields number was calculated using the formula of Soulsby and Whitehouse (1997) and the bed shear stress was corrected for sidewall effects (Vanoni & Brooks, 1957; Chiew & Parker, 1994). Since no value was given regarding the bed state, a bed roughness length of $z_0 = 3\,d_{90}/30$ was chosen (van Rijn, 1982). Although the dimensions of the flume used in the experiment are not indicated, we make the assumption that all grain sizes were at saturation since the transport lengths, up to 1 cm, are very short. Figure 7b shows the comparison between the transport capacities predicted by our model and the experimental values of Meyer-Peter and Müller (1948). Model predictions are slightly poorer as 74% and 80% of the experimental data are predicted within a factor of 5 and 10, respectively. Considering only the uniform sediment (5.21-mm and 28.65-mm grain sizes), 87% and 94% of the experimental data are predicted within a factor of 5 and 10, respectively. Large incorrect predictions in the vicinity of the threshold of motion are likely related to incorrect estimates of θ_c, as we have to infer it, and cannot properly account for

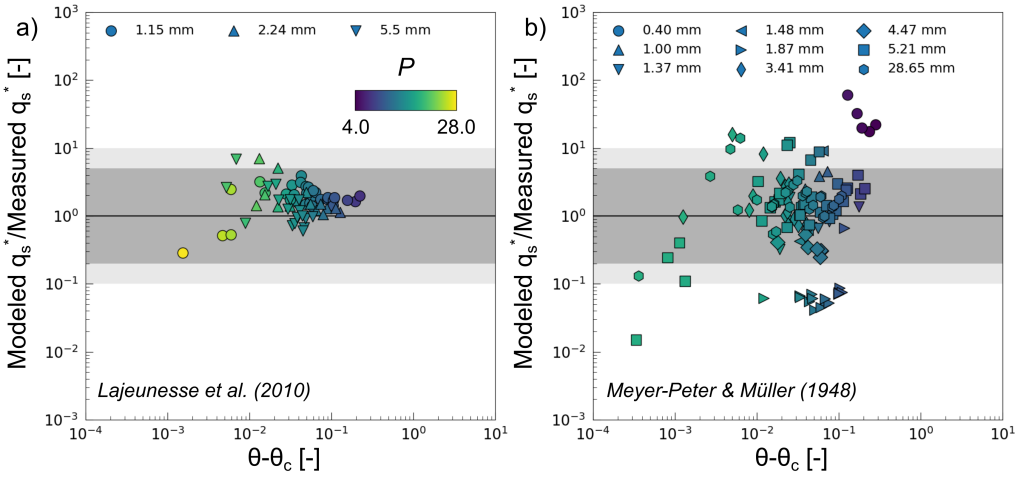

Figure 7. Predictions of bed load transport rates at equilibrium for single grain sizes. Model predictions compared to flume observations by Lajeunesse et al. (2010; a) and Meyer-Peter & Müller (1948; b). The dark and light gray areas correspond to measured values that are predicted within a factor of 5 and 10, respectively.

bedforms or sediment heterogeneity. Similarly, using the skin-related shear stress instead of the total shear stress could improve model predictions, but would require additional model complexity.

Second, we examine our model predictions for bed load experiments considering a spectrum of grain sizes. We compare the dimensionless fractional bed load transport capacities predicted by our model to the data of Houssais and Lajeunesse (2012) and Wilcock et al. (2001). We used the data available for the following parameters: water discharge, water depth, hydraulic slope, sediment surface fraction, transport fraction, sediment load, and sediment diameter. For the comparison with Houssais and Lajeunesse (2012), we used the critical threshold of motion that they measured (Table 2 in their paper) and a bed roughness length of $z_0 = 3\,d_{50}/30$ was assumed. All grain sizes were at saturation since the transport lengths up to 2 mm are very short compared to the 2-m-long flume working section down stream. Figure 8a shows that the magnitude of the dimensionless modeled transport capacities are in good agreement with the experimental values of Houssais and Lajeunesse (2012): 95% and 96% of the experimental data are predicted by our model within a factor of 5 and 10, respectively. As stated before, our model calibration may explain these good results. For the comparison with the data of Wilcock et al. (2001), a bed roughness length

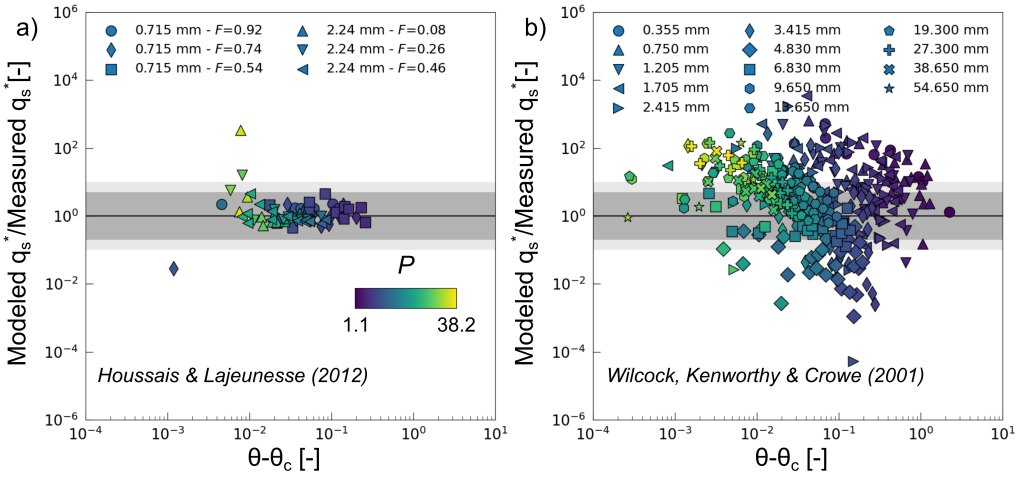

Figure 8. Predictions of bed load transport rates at equilibrium for mixtures. Model predictions compared to flume observations by Houssais and Lajeunesse (2012; a) and Wilcock, Kenworthy & Crowe (2001; b). The dark and light gray areas correspond to measured values that are predicted within a factor of 5 and 10, respectively.

of $z_0 = 3\,d_{90}/30$ was assumed. The same method as the one mentionned in Wilcock and Crowe (2003) was applied to calculate values of bed shear stress corrected for sidewall effects (Vanoni & Brooks, 1957; Chiew & Parker, 1994). We used the bed-surface grain size reported by Wilcock et al. (2001) for each size and each transport sample to specify F_i, to estimate the critical shear stress corrected from hiding-exposure effects $\tau_{c,i}$ (Equations 4 and 6 in Wilcock and Crowe (2003)) and ultimately to calculate the grain-size specific erosion rate $\dot{e}_i$. All grain sizes were at saturation since the transport lengths up to 1 cm are very short compared to the 8-m-long flume working section down stream. Figure 8b shows that the model predicts transport capacities which are on average consistent with the experimental data of Wilcock et al. (2001). However, the model overpredicts fluxes at low excess Shields number, and underpredict them at high excess Shields numbers up to two orders of magnitude. The evaluation of the fit of the transport capacity as a function of excess Shields number gives 36% and 50% of the experimental data that are predicted by our model within a factor of 5 and 10, respectively. We explore the potential causes of the poorer prediction results of the model in the discussion.

4.2.2 Total load transport

Total load transport formulas predict stream capacities that combine all modes of transport. Modeled transport capacities fall within the range of magnitudes reported in literature (Bagnold, 1966; Engelund & Hansen, 1967; van Rijn, 1984b). They exhibit a scaling that spreads from 2.1 to 2.8 for $5 \times 10^{-1} < \theta - \theta_c < 10^1$ and thus appears to vary around the value of 2.5 found by Engelund and Hansen (1967) (Figure 6).

For further assessment of the performance of our model in terms of magnitude, we compare the magnitudes of transport capacities predicted by our model to flume measurements. To do so, the data used by Engelund and Hansen (1967) were extracted from the report by Guy et al. (1966). Parameters such as water depth, water discharge, flume width, sediment grain size, sediment load serve as inputs for our calculations. The critical Shields number was calculated using the formula of Soulsby and Whitehouse (1997) and the bed shear stress was corrected for sidewall effects (Vanoni & Brooks, 1957; Chiew & Parker, 1994). The state of the bed was described for some of the experiments but lacking for others. When the state of the bed is not described, we assume the bed to be plane with a roughness length of $z_0 = 3\,d_{90}/30$ (van Rijn, 1982). When sand dunes are reported along with their height H_s [m] and length L_s [m], we consider the roughness length to be $z_0 = max\left(3\,d_{90}/30, 8\,\frac{H_s^2}{L_s}\right)$ since it gives the best results with our model (Nielsen, 1992). All grain sizes were at saturation since the transport lengths up to 24 cm are very short compared to the 45-m-long flume. Figure 9 shows the comparison between the total transport capacities predicted by our model and the experimental values of Guy et al. (1966). The model predicts 51% and 66% of the total transport capacities within a factor of 5 and 10, respectively (Figure 9). This is obtained without calibration of the model in the "suspension" regime.

The discrepancy between predictions and observations is likely to stem from the measurements of the sediment load since local changes in bed shear stress and turbulences may have caused a strong variability in sampled concentration of suspended sediment (Guy et al., 1966). Another parameter that may play a role is the bed roughness length z_0 associated with the presence of dunes affecting the velocity profile.

5 Sensitivity analysis

The following sensitivity analysis was conducted to understand how the different parameters of our model impact the predictions of transport length and transport capacity and

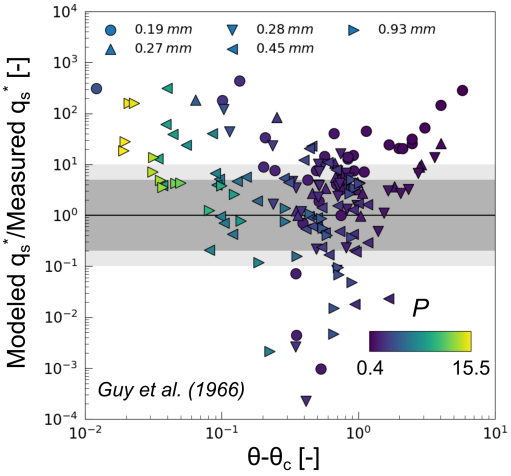

Figure 9. Predictions of total load transport rates at equilibrium for single grain sizes. Model predictions compared to flume observations by Guy et al. (1966). The dark and light gray areas correspond to measured values that are predicted within a factor of 5 and 10, respectively.

identify key variables that should be measured beforehand and those that do not require a precise parametrization.

5.1 Diffusivity ratio

The diffusivity ratio β gives shape to the vertical sediment concentration profile via the modified Rouse number (Equations 11 and 12). It affects the characteristic transport height h_s by controlling the gradient of vertical sediment distribution in the water column r_0 (Equations 10 and 13). Thus the diffusivity ratio plays a role in the transport length ξ (Equation 8) and the deposition rate $\dot{d}$ for sediment transported in suspension (Equation 7). Tests reveal that a change in the ratio of sediment diffusivity to eddy viscosity influences the deposition rate predictions far from the threshold of motion but has only limited effect in its vicinity (Figure 10a). Different formulas exist to calculate the diffusivity ratio (Rouse, 1937; van Rijn, 1984b; Rose & Thorne, 2001; Cheng et al., 2013; Santini et al., 2019; Chauchat et al., 2022). Rose and Thorne (2001) established that this ratio varies between 0 and 3.1 and increases with a decreasing ratio of the shear velocity to the settling velocity. Santini et al. (2019) modified the equation proposed by Rose and Thorne (2001) to account for the change in sediment distribution through the water column due to water depth. These two formulas lead to longer modeled transport lengths and thus lower deposition rates at large excess

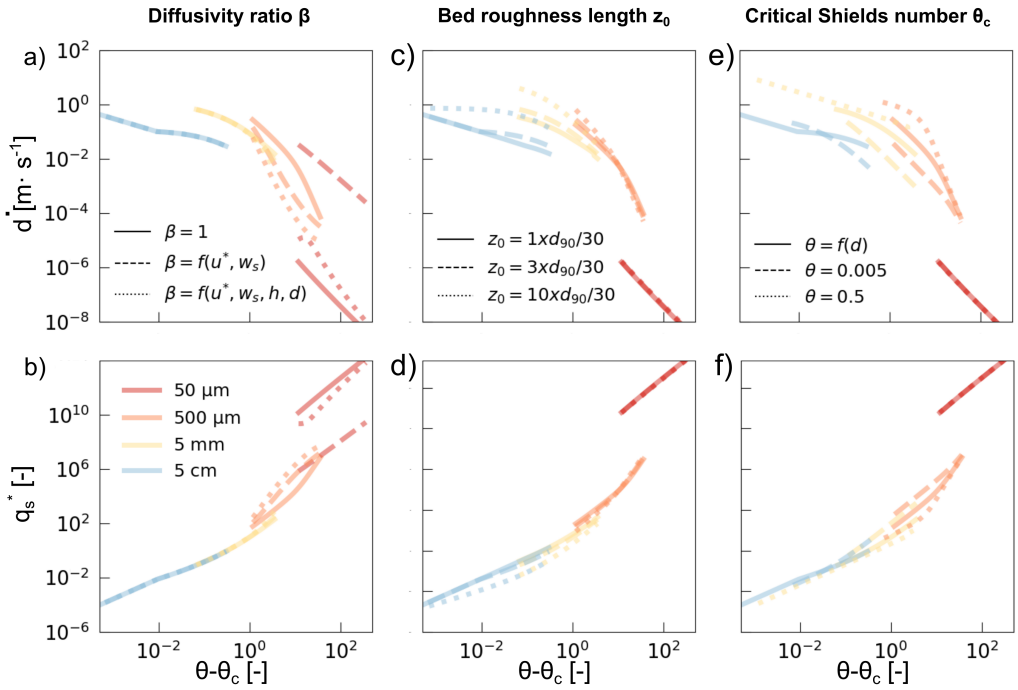

Figure 10. Sensitivity analysis of the Multi Grain-Size Total Load Sediment Transport Model. The effect on the deposition rate via the transport length (upper row) and transport capacity (lower row) of three parameters was tested: a-b) diffusivity ratio β, c-d) bed roughness length z_0, e-f) threshold of motion θ_c. Three formulas of the diffusivity ratio were tested: $\beta = 1$ (Rouse, 1937), $\beta = f(u^*, w_s)$ (Rose & Thorne, 2001) and $\beta = f(u^*, w_s, h, d)$ (Santini et al., 2019). Three values of bed roughness length were tested according to the ones reported in van Rijn (1984a). Three formulas of critical Shields number were tested: Soulsby and Whitehouse (1997) ($\theta_c = f(d)$), θ_c=0.005 and θ_c=0.5.

Shields number when $\beta < 1$ (Figure 10a). Consequently, variations in diffusivity ratio affect predictions of suspended load transport rates but not bed load transport rates (Figure 10b). Indeed, at large excess Shields number, the scaling of the dimensionless transport capacity increases with decreasing diffusivity ratio and the magnitude of the dimensionless transport capacity rises.

5.2 Bed roughness length

The bed roughness length z_0 calculated using the bed roughness height k_s is considered as the reference height of the parabolic velocity profile. This parameter is used to calculate the characteristic height h_s via the vertical gradient of sediment distribution r_0 which plays

a role for suspended sediment (Equations 10 and 13) and to compute the characteristic velocity $\overline{v}_s$ (Equation 16). Consequently, the bed roughness length plays a role in the transport length ξ (Equation 8) and the deposition rate $\dot{d}$ (Equation 7) for all transport modes. Figure 10c shows that a change in bed roughness height affects the deposition rate predictions in the vicinity of the threshold of motion but has only limited impact away from it. Consequently, it mostly affects bed load transport predictions. Indeed, a decrease in bed roughness height from $k_s = 10\, d_{90}$ to $k_s = d_{90}$ is associated with an increase in the modeled transport lengths and thus a decrease in deposition rates at low excess Shields number (Figure 10c). We note that having bed roughness explicitely in the model allows to potentially account for the presence of bed forms, for which formulas exist (van Rijn, 1982, 1984c; Grant & Madsen, 1986; Nielsen, 1992). At low excess Shields number, the scaling of the dimensionless transport capacity decreases slightly with higher bed roughness height and the magnitude of the dimensionless transport capacity decreases (Figure 10d).

5.3 Threshold of motion

The transport stage T^* influences the characteristic transport height h_s (Equation 10) and, in turns, the characteristic transport velocity $\overline{v}_s$ in the saltation regime (Equation 16). Thus, the critical shear stress τ_c beyond having an explicit role in the erosion rate (Equation 3), also has an implicit contribution to the deposition rate $\dot{d}$ through the transport length ξ (Equations 7 and 8). A change in the threshold of motion affects the deposition rate and erosion rate (not shown here) predictions, with the largest variations in rate occurring close to the threshold. Indeed, the modeled deposition rates increase with increasing critical Shields number (Figure 10e). Ultimately, variations in threshold of motion affect bed load predictions by several orders of magnitudes (Figure 10f). The grain-size specific threshold of motion is a critical parameters to tune when predicting bedload transport capacities. Note that the critical shear stress may also vary with the bed slope (Recking, 2009).

6 Discussion about the continuous model of sediment transport

6.1 Transport length

Our continuous model of sediment transport length covers the full spectrum of transport modes from rolling or sliding to suspension, passing by saltation. The power of this Multi-Mode Transport Length model is due to a single parameter: the characteristic transport

height h_s. h_s brings physical consistency by representing sediment motion as a continuum of motion and thus enhances the richness of sediment transport prediction for an heterogeneous population of sediment grains. This parameter is the key to the unified theory of sediment transport since it includes the complexity of all the transport modes with dependencies on sediment properties and hydraulic conditions (water discharge, slope).

The transport length varies strongly non-linearly with grain size and is affected by the slope for fine grains transported in suspension only (Figures 5b and 11a). Such a large dispersion of transport lengths may play an important role in the generation of anomalous diffusion for populations of heterogeneous sediments (Martin et al., 2012). The new model predicts disequilibrium lengths ξ that do not identify with published equations of saltation and suspension lengths. Using the latter values would lead to significant over-estimation of transport capacities.

6.2 Single grain-size transport law

Our model is able to predict the transport capacity across a wide range of transport stages, and manages to seize the two transport law scalings with the shear stress regularly reported in the literature: $m \approx 1.5$ for bed load transport (Meyer-Peter & Müller, 1948) and $m \approx 2.5$ for total load transport (Engelund & Hansen, 1967). Our model is locally consistent with existing transport law scalings but differs also from them since the scaling continuously varies with the transport stage (Figures 6 and 11b). Since the erosion rate increases linearly with increasing shear stress, changes in scaling of the stream capacities with the shear stress stem from the variations in the magnitude of transport length. More precisely, the change in scaling mainly comes from the characteristic transport height h_s and the fact that the contribution of the suspension prevails on the saltation in Equation 10. As h_s continuously changes with T^*, so does the scaling exponent.

We can explore asymptotic behaviors to understand the origin of the scaling exponents.

- In the vicinity of the threshold of motion, sediment tend to be transported in saltation as bed load. When the characteristic height (Equation 10) is independent of the shear stress, $h_s \approx 0.6\, d \propto \tau^0$, the characteristic velocity scales with the shear stress as $\overline{v}_s \propto T^*$ or $u^* \propto \tau^{0.5}$ (Equation 16). Consequently, the transport length scales with the bed shear stress as $\xi \propto \tau^{0.5}$ resulting in a saturated flux scaling as $\tau^{1.5}$, which is similar to the formula derived by Meyer-Peter and Müller (1948). With

increasing shear stress during bed load transport, a second regime of saltation height takes place. The characteristic height (Equation 10) scales with the shear stress as $h_s \approx 0.6\,d + 0.025\,d\,T^* \propto \tau^1$, while the characteristic velocity still depends on the shear stress as $\overline{v}_s \propto \tau^{0.5}$ (Equation 16). Consequently, the transport length scales with the bed shear stress as $\xi \propto \tau^{1.5}$ resulting in a saturated flux scaling as $\tau^{2.5}$, which is similar to the formula derived by Engelund and Hansen (1967).

- Far from the threshold of motion, sediment tend to be transported as suspended load in a layer with a thickness that tends towards the water depth h. While the characteristic height (Equation 10) has a linear dependency on the shear stress $h_s \approx h \propto \tau^1$, the characteristic velocity (Equation 16) is about the depth-averaged flow velocity $\bar{u}$ and thus scales with the shear stress as $\overline{v}_s \propto \tau^{0.5}$. Therefore, the associated transport length scales with the bed shear stress as $\xi \propto \tau^{1.5}$ which results in a saturated load scaling as $\tau^{2.5}$ similar to the formula derived by Engelund and Hansen (1967).

It appears that two modes of transport lead to a scaling of 2.5 of the total load with the bed shear stress. Scaling values between the saltation and the suspension regimes may be larger than 2.5 (Figure 11b) since it corresponds to a transition phase between the two transport modes, when the gradient of sediment distribution r_0 has a non-zero scaling with the shear stress. For fine grains, the transition between the 1.5 and 2.5 scaling exponents is sensitive to the bed slope (Figure 11b) with scaling values that increase (above 2.5) with decreasing slope.

The equilibrium transport rate equation that stems from our new transport length formulation combined to the erosion-deposition framework can be simply expressed for spherical grains. Although our model has no free parameter but rather uses relations deduced from experimental measurements carried out in very variable conditions, it yet succeeds in predicting transport capacities consistent with the existing single grain-size laws and for a wide range of grain sizes and transport rates. Indeed, the erosion coefficient k_e equation derived from Lajeunesse et al. (2010) and Houssais and Lajeunesse (2012) appears to reasonably predict the erosion rate for the single grain-size approach when grains are transported as bed load. Further tests should be carried out to examine the effects of non-spherical grains, large sediment concentrations, grain collisions, etc., on this entrainment coefficient. Furthermore, the sensitivity analyses reveal that some parameters critically affect model

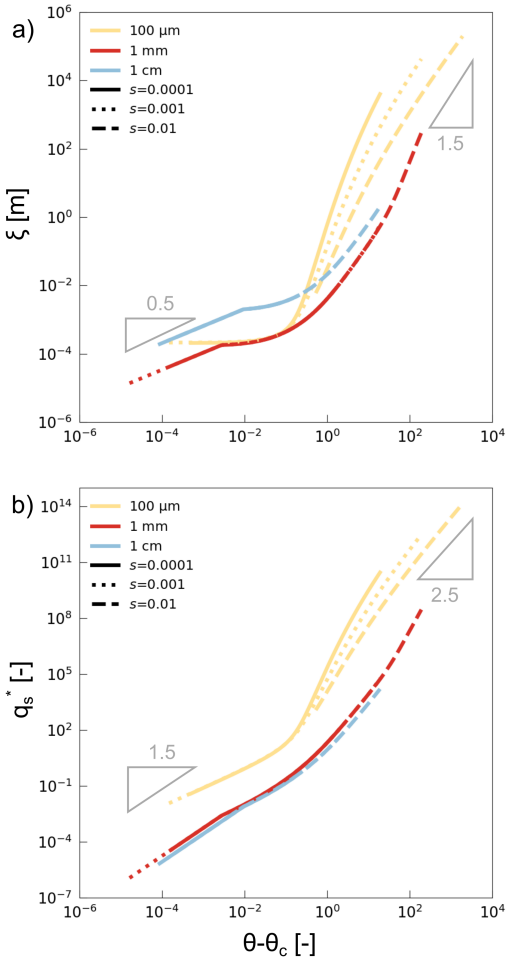

Figure 11. Predictions of transport lengths and transport rates at equilibrium. a) Transport length ξ plotted against the dimensionless excess of shear stress $\theta - \theta_c$. b) Dimensionless transport capacity q_s^{eq*} plotted against the dimensionless excess of shear stress $\theta - \theta_c$. A grain diameter of 500 µm, a hydraulic slope of 0.001 and a water depth ranging from 1 cm to 30 m were considered. The bed roughness was taken as $z_0 = 3d_{90}/30$.

predictions and thus should be carefully chosen. Bed load predictions are affected by the threshold of motion θ_c and impacted by the bed roughness length z_0 through the characteristic velocity of transport $\overline{v}_s$. The bed roughness length z_0 calculated using bedform height and length or assumed as $z_0 = 3\,d_{90}/30$ may differ from the actual one. Under-estimating the bed roughness length results in predicted transport capacities much greater than the measured ones. Besides, the threshold of motion obviously influences the modeled transport lengths and thus transport capacities to a small extent.

For suspended load, our model over-estimates the transport capacities predicted by van Rijn (1984b) (Figure 6) and measured by Guy et al. (1966) (Figure 9). For $\theta - \theta_c > 1$, the increasing trend may be caused by the approximation we make to calculate the gradient of distribution r_0. This gradient writes without approximation as $r_0 = C_s\,h/h_s\;(q - q_{salt})\,/\,(q_s - q_{s,salt})$. However, we assume that fluxes related to the saltation layer q_{salt} and $q_{s,salt}$ are negligible compared to fluxes over the whole water column for sediment in suspension and thus that the gradient of sediment distribution writes $r_0 \approx h/h_s$. This may be a too gross approximation that results in under-estimation of this gradient and thus in predicted transport capacities much greater than observed ones. Besides, suspended/total load predictions are influenced by the diffusivity ratio β that determines the distribution of the sediment over the water column. In addition, we use the total shear stress instead of the skin- and bedform-related shear stresses to predict the bed load and suspended load, respectively. Thus, the associated shear stress may be wrongly estimated since it does not account for the presence of bedforms and thus causes over-/under-predictions of transport capacities.

6.3 Extension to a multi grain-size model

The model presented before can be extended to a population of grains with various sizes by considering the grain-size specific deposition rate $\dot{d}_i = q_{s,i}/\xi_i$ and the grain-size specific erosion rate $\dot{e}_i = F_i\,k_{e,i}\;(\tau - \tau_{c,i})$ where F_i [-] is the grain-size specific fraction and by accounting for the effects of grain interactions on the grain-size specific threshold of motion.

In contrast to monodisperse sediment, grains in sediment mixtures are subject to different drag forces that control their mobility (Einstein, 1950). Indeed, hiding effects that occur when fine grains are sheltered behind coarser grains lead to an increase in bound-

ary shear stress required to move fine grains. This boundary shear stress is closer to the value of boundary shear stress needed to initiate motion of coarse grains. Similarly, coarse grains protude through the surface and are more exposed to the flow, meaning that exposure effects lead to a decrease in boundary shear stress required to move coarse grains. As a consequence, the critical boundary shear stress $\tau_{c,i}$ is corrected to account for these hiding-exposure effects.

Empirical equations (Einstein, 1950; Wilcock, 1993) express the corrected critical shear stress as:

$$\tau_{c,i} = \zeta_i \, \tau_{c,50} \quad \text{where} \quad \zeta_i = \left(\frac{d_i}{d_{50}} \right)^{1-\gamma} \tag{25}$$

where ζ_i [-] is the empirical factor of hiding-exposure, $\tau_{c,50}$ $[Pa]$ is the critical shear stress associated to the median diameter $d_{50}[m]$ of the sediment mixture and $\gamma[-]$ is the exponent of hiding-exposure independent of the grain size ($0 \leq \gamma \leq 1$; Parker and Toro-Escobar (2002)). Equation 25 is generic enough to capture asymptotic behaviours in which hiding-exposure effects dominate or not. An exponent $\gamma = 0$ to the case when they are no hiding-exposure effects, while an exponent of $\gamma = 1$ means equal mobility, i.e., all grains sizes in a mixture have the critical shear stress of the median grain size.

Contrary to the previous equation that assumes fine grains sitting on coarser grains and that does not consider bed armouring, the theoretical formula of Egiazaroff (1965) could be used to calculate the factor of hiding-exposure ζ_i:

$$\zeta_i = \left(\frac{\log_{10}(19)}{\log_{10}(19 d_i / d_{50})} \right)^2 \tag{26}$$

Wilcock and Crowe (2003) suggests another approach to estimate the grain-size specific critical shear stress that fundamentally differs from the power law relationship (Equation 25) and the Egiazaroff function (Equation 26). They established a model of hiding-exposure factor that has the form of a power function but with an exponent γ_i that depends on the grain size:

$$\gamma_i = 1 - \frac{0.67}{1 + \exp\left(1.5 - \frac{d_i}{d_{50}}\right)} \tag{27}$$

This hiding function reveals the grain-size sorting that occurs between the bed surface and the subsurface through the d_i/d_{50} ratio as well as the impact of the sand fraction on the bed mobility.

It is worth noting that the model presented in this paper is based on equations established for sediment of single size. Thus, all the processes associated with sediment mixture of various sizes are likely not encompassed in the current formulation of both the characteristic transport height h_s and the erosion coefficient k_e. This likely explains why the application of the model to the Wilcock et al. (2001) experiments shows residuals that are strongly correlated with the transport stage. This trend may emerge from the definition of the saltation height $h_{salt} \approx 0.6\,d$ for very low excess Shields numbers. At a given excess Shields number, this leads to higher saltation heights for coarse grains and smaller saltation heights for fine grains. This may be counterintuive for a population of grain transported simultaneously, and does result in a decreasing trend in the predicted transport capacities with excess Shields number. In the absence of theoretical or experimental data describing h_s for strongly heterogeneous sediment mixtures, we hypothetise that h_s should depend on an effective grain size, or measure of the bed roughness. For instance, modifying the first right-member of the equation of Auel et al. (2017) by using the median diameter: $h_{salt} = 0.6\,d_{50} + a\,d\,T^{*b}$, removes the decreasing trend. A significant offset exists between the predicted and observed bedload fluxes, that can be compensated by reducing the coefficient of erosion k_e by a factor three (Figure 12). This results in 39% and 57% of the experimental data that are predicted by our model within a factor of 5 and 10, respectively. Indeed, if the critical shear stress of entrainment must be adjusted for a population of grains, it is very likely that the coefficient of erosion may also depends on hiding-exposure effects that are yet to fully comprehend. If Equations 25, 26 and 27 are indicative of the level of complexity needed to account for hiding-exposure effect, we do expect that h_s and k_e may have potentially complex formulations. The above tweak of Eq. 9 and k_e is only indicative that the new framework we propose may offer generalization between single grain-size and multi grain-size total load transport in a complete new way, bringing us closer to a universal sediment transport model, both in stationary and non-stationary conditions.

7 Conclusions

Despite numerous sediment transport formulas, none is applicable for both bed load and suspended load while also considering sediment heterogeneity and various flow conditions.

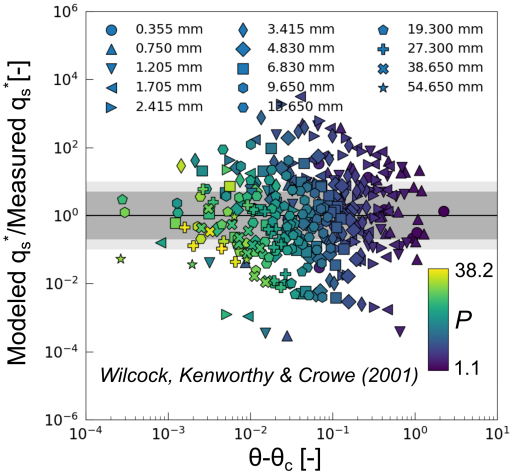

Figure 12. Adjusted predictions of bed load transport rates at equilibrium for flume observations by Wilcock et al. (2001). A modified version of Eq. 9, $h_{salt} = 0.6\,d_{50} + a\,d\,T^{*b}$, was used as well as an erosion coefficient k_e three times smaller. The dark and light gray areas correspond to measured values that are predicted within a factor of 5 and 10, respectively.

The combination of the transport length model with the erosion-deposition framework leads to the emergence of a continuous theory of sediment transport that may be applied for a wide range of shear stresses and sediment mixtures.

We present a continuous model of sediment transport length that depends on three parameters: a characteristic height, a characteristic velocity and a settling velocity. The former two relates to the portion of the water column where most of the sediment fluxes occurs. The characteristic height is the key parameter that encompasses the diversity of transport modes while the characteristic velocity includes the influence of bed properties such as the bed roughness that is highly sensitive to the granulometry and the state of the bed, e.g., bed forms. Hence, the transport length embraces the variety of physical processes that govern grain motion as a continuum. To our knowledge, this is one of the first models that attempts to capture all the modes of transport, i.e., rolling, saltation and suspension, for a population of heterogeneous grains regardless of the water discharge.

The new parametrization of the transport length combined to the erosion-deposition framework allows for the calculation of equilibrium transport rates, i.e., stream capacities. Our continuous transport model is applied to both bed load and suspended load thanks to the transport length that dictates how the transport rate scales with the bed shear stress.

Besides, the Multi-Mode transport length model we developed could be a powerful tool to study sediment mixtures when different modes of transport may be observed simultaneously. The adaptation of the erosion-deposition framework for multi grain-size transport is done by considering hiding-exposure effects and sediment fractions but adjustment are needed to have a fully functional model for sediment mixtures. Its application in the context of channel morphodynamics would require an additional component that accounts for grain size sorting between the transport, the bed surface, and the bed subsurface.

Appendix A Computation of deposition and erosion rates

The input data required to compute the deposition and erosion rates are: the sediment grain diameter d, the sediment diffusivity ratio β, the sediment density ρ_s, the sediment settling velocity w_s, the sediment Shields number θ_c, the water depth h, the sediment flux q_s (for non-stationary conditions) the water density ρ, the hydraulic slope s, the depth-averaged water velocity $\overline{u}$,the channel width W and the bed roughness length z_0. The value of three constants such as the gravitational constant g, the von Karman constant κ and the empirical constant for the erosion coeffcient c_e are also needed.

The computation of the deposition rate is as follows:

1. compute the bed shear stress τ as $\tau = \rho\, g\, R_h\, s$ where $R_h = hW/\left(2h + W\right)$ is the hydraulic radius;
2. compute the critical shear stress τ_c according to Soulsby and Whitehouse (1997) and potentially corrected from hiding-exposure effects in the case of multi grain sizes;
3. compute the erosion coefficient k_e using Equation 4;
4. compute the erosion rate $\dot{e}$ using Equation 3.

The computation of the deposition rate is as follows:

1. compute the bed shear stress τ as $\tau = \rho\, g\, R_h\, s$ where $R_h = hW/\left(2h + W\right)$ is the hydraulic radius;
2. compute the critical shear stress τ_c according to Soulsby and Whitehouse (1997) and potentially corrected from hiding-exposure effects in the case of multi grain sizes;
3. compute the transport stage T^* as $T^* = \tau/\tau_c - 1$;
4. compute the saltation height h_{salt} using Equation 9;
5. compute the shear velocity u^* as $u^* = \sqrt{\tau/\rho}$;
6. compute the Rouse number P using Equation 12;
7. compute the distribution gradient r_0 using Equation 13;
8. compute the characteristic transport height h_s using Equation 10;
9. compute the saltation velocity v_{salt} using Equation 14;
10. compute the average water velocity in the transport layer v_{layer} using Equation 15;
11. compute the characteristic transport velocity $\overline{v}_s$ using Equation 16;
12. compute the disequilibrium length ξ using Equation 8;

765 13. compute the deposition rate $\dot{d}$ using Equation 7.

766 The stationary total sediment load is obtained as $q_s^{eq} = \xi\, \dot{e}$ (Equation 17).

Notation

$\boldsymbol{a}$: factor for the saltation height

$\boldsymbol{\alpha}$: empirical constant for the saltation height

$\boldsymbol{b}$: exponent for the saltation height

$\boldsymbol{\beta}$: diffusivity coefficient

$\boldsymbol{c_e}$: empirical constant for the erosion coefficient

$\boldsymbol{C_s}$: sediment concentration

$\boldsymbol{C_{s,ref}}$: sediment concentration at the reference height

$\boldsymbol{C_s^*}$: sediment concentration in the layer of transport

$\boldsymbol{d}$: sediment grain diameter

$\boldsymbol{d_{50}}$: median diameter

$\boldsymbol{d_{90}}$: 90% of the grains are smaller than this diameter

$\boldsymbol{\dot{d}}$: deposition rate

$\boldsymbol{\dot{e}}$: erosion rate

$\boldsymbol{F}$: surface volume fraction

$\boldsymbol{g}$: gravitational constant ($9.81\, m \cdot s^{-2}$)

$\boldsymbol{\gamma}$: exponent of hiding-exposure

$\boldsymbol{h}$: water depth

$\boldsymbol{h_s}$: characteristic sediment transport height

$\boldsymbol{h_{salt}}$: saltation height

$\boldsymbol{\kappa}$: von Kármán constant

$\boldsymbol{k_e}$: erosion coefficient

$\boldsymbol{k_s}$: roughness height

$\boldsymbol{l_{salt}}$: saltation length

$\boldsymbol{l_{susp}}$: suspension length

$\boldsymbol{m}$: scaling of the transport rate with bed shear stress

$\boldsymbol{\nu}$: kinematic viscosity of water ($10^{-6}\, m^2 \cdot s^{-1}$)

$\boldsymbol{n}$: surface density of moving particles

$\boldsymbol{\dot{n_e}}$: erosion rate

$\boldsymbol{\dot{n_d}}$: deposition rate

$\boldsymbol{P}$: Rouse number

$\boldsymbol{q}$: water discharge per unit width

$\boldsymbol{q_s}$: sediment load in the stream per unit width

$\boldsymbol{q_s^{eq}}$: transport capacity

$\boldsymbol{q_s^*}$: dimensionless transport rate

$\boldsymbol{R}$: sediment specific gravity

$\boldsymbol{r_0}$: gradient of sediment distribution above the saltation layer

$\boldsymbol{\rho}$: water density ($1\,000\,kg \cdot m^{-3}$)

$\boldsymbol{\rho_s}$: sediment density ($2\,650\,kg \cdot m^{-3}$ unless mentionned otherwise)

$\boldsymbol{t_d}$: deposition time

$\boldsymbol{t_e}$: erosion time

$\boldsymbol{T^*}$: transport stage

$\boldsymbol{\tau}$: bed shear stress

$\boldsymbol{\tau_c}$: critical shear stress

$\boldsymbol{\theta}$: Shields number

$\boldsymbol{\theta_c}$: critical Shields number

$\boldsymbol{\theta_{c,50}}$: critical Shields number for the d_{50}

$\boldsymbol{u}$: average flow velocity

$\boldsymbol{u^*}$: shear velocity

$\boldsymbol{v_{layer}}$: average water velocity in the transport layer

$\boldsymbol{\overline{v}_s}$: characteristic sediment transport velocity

$\boldsymbol{v_{salt}}$: saltation velocity

$\boldsymbol{w_s}$: sediment settling velocity

$\boldsymbol{\xi}$: sediment transport length

$\boldsymbol{z_0}$: roughness length

$\boldsymbol{z_{ref}}$: reference height of the Rouse profile

$\boldsymbol{\zeta}$: hiding-exposure factor

Acknowledgments

The authors are grateful to the reviewers for their valuable comments to improve the quality of the manuscript. This work has been funded by the Brittany Regional Council (France) through the SAD/SEDRISK project and by the New Zealand Governments Ministry of

Business, Innovation and Employment's Endeavour fund as part of the work carried out for the Earthquake Induced Landscape Dynamics programme (C05X1709).

Data availability statement

Data tables and Python scripts that support the findings of this study are available in a Zenodo repository at (Le Minor et al., 2022): https://doi.org/10.5281/zenodo.7221833.

References

Ackers, P., & White, W. R. (1973). Sediment Transport: New Approach and Analysis. *Journal of the Hydraulics Division*, *99*(11), 2041-2060. doi: 10.1061/JYCEAJ.0003791

Ali, S. Z., & Dey, S. (2019). Bed Particle Saltation in Turbulent Wall-Shear Flow: A Review. *Proceedings of the Royal Society A: Mathematical, Physical and Engineering Sciences*, *475*(2223), 20180824. doi: 10.1098/rspa.2018.0824

Ashida, K., & Michiue, M. (1973, jan). Studies on Bed-Load Transport Rate in Open Channel Flows. In *Proceedings of the International Association for Hydraulic Research International Symposium on River Mechanics, Bangkok, Thailand* (p. 407417).

Auel, C., Albayrak, I., Sumi, T., & Boes, R. M. (2017). Sediment Transport in High-Speed Flows Over a Fixed Bed: 1. Particle Dynamics. *Earth Surface Processes and Landforms*, *42*(9), 1365-1383. doi: 10.1002/esp.4128

Bagnold, R. A. (1966). *An Approach to the Sediment Transport Problem from General Physics, U.S. Geol. Surv. Prof. Pap., 422-i.* US government printing office.

Camenen, B., & Larson, M. (2008, 05). A General Formula for Noncohesive Suspended Sediment Transport. *Journal of Coastal Research*, *24*(3 (243)), 615-627. doi: 10.2112/06-0694.1

Charru, F. (2006). Selection of the Ripple Length on a Granular Bed Sheared by a Liquid Flow. *Physics of Fluids*, *18*(12), 121508. doi: doi.org/10.1063/1.2397005

Charru, F., Mouilleron, H., & Eiff, O. (2004). Erosion and Deposition of Particles on a Bed Sheared by a Viscous Flow. *Journal of Fluid Mechanics*, *519*, 5580. doi: 10.1017/S0022112004001028

Chauchat, J., Hurther, D., Revil-Baudard, T., Cheng, Z., & Hsu, T.-J. (2022). Controversial Turbulent Schmidt Number Value in Particle-Laden Boundary Layer Flows. *Phys. Rev. Fluids*, *7*, 014307. doi: 10.1103/PhysRevFluids.7.014307

Cheng, C., Song, Z.-Y., Wang, Y.-G., & Zhang, J.-S. (2013). Parameterized Expressions

for an Improved Rouse Equation. *International Journal of Sediment Research*, *28*(4), 523-534. doi: 10.1016/S1001-6279(14)60010-X

Chiew, Y.-M., & Parker, G. (1994). Incipient sediment motion on non-horizontal slopes. *Journal of Hydraulic Research*, *32*(5), 649-660. doi: 10.1080/00221689409498706

Daubert, A., & Lebreton, J. (1967). Étude Expérimentale et sur Modèle Mathématique de Quelques Aspects du Calcul des Processus d'érosion des Lits Alluvionaires en Régime Permanent et Non Permanent. In *Proceedings of the 12th Congress of IAHR, Fort Collins, CO, USA* (pp. 11–14).

Davy, P., & Lague, D. (2009). Fluvial Erosion/Transport Equation of Landscape Evolution Models Revisited. *Journal of Geophysical Research: Earth Surface*, *114*(F3). doi: 10.1029/2008JF001146

de Leeuw, J., Lamb, M. P., Parker, G., Moodie, A. J., Haught, D., Venditti, J. G., & Nittrouer, J. A. (2020). Entrainment and Suspension of Sand and Gravel. *Earth Surface Dynamics*, *8*(2), 485–504. doi: 10.5194/esurf-8-485-2020

Egiazaroff, I. V. (1965). Calculation of Nonuniform Sediment Concentrations. *Journal of the Hydraulics Division*, *91*(4), 225-247. doi: 10.1061/JYCEAJ.0001277

Einstein, H. A. (1950). *The Bed-Load Function for Sediment Transportation in Open Channel Flows* (No. 1026). United States Department of Agriculture, Soil Conservation Service, Washington, DC.

El kadi Abderrezzak, K., & Paquier, A. (2009). One-dimensional Numerical Modeling of Sediment Transport and Bed Deformation in Open Channels. *Water Resources Research*, *45*(5). doi: 10.1029/2008WR007134

Engelund, F., & Fredse, J. (1976, 10). A Sediment Transport Model for Straight Alluvial Channels. *Hydrology Research*, *7*(5), 293-306. doi: 10.2166/nh.1976.0019

Engelund, F., & Hansen, E. (1967). *A Monograph on Sediment Transport in Alluvial Streams* (Tech. Rep.). Technical University of Denmark.

Fernandez-Luque, R., & Beek, R. V. (1976). Erosion and Transport of Bed-Load Sediment. *Journal of Hydraulic Research*, *14*(2), 127-144. doi: 10.1080/00221687609499677

Galappatti, G., & Vreugdenhil, C. B. (1985). A Depth-integrated Model for Suspended Sediment Transport. *Journal of Hydraulic Research*, *23*(4), 359-377. doi: 10.1080/00221688509499345

Ganti, V., Lamb, M., & McElroy, B. (2014). Quantitative Bounds on Morphodynamics and Implications for Reading the Sedimentary Record. *Nature Communications*, *5*(3298).

doi: 10.1038/ncomms4298

Garcia, M., & Parker, G. (1991). Entrainment of Bed Sediment into Suspension. *Journal of Hydraulic Engineering*, *117*(4), 414-435. doi: 10.1061/(ASCE)0733-9429(1991)117:4(414)

Graf, W., & Cellino, M. (2002). Suspension Flows in Open Channels; Experimental Study. *Journal of Hydraulic Research*, *40*(4), 435-447. doi: 10.1080/00221680209499886

Grant, W. D., & Madsen, O. S. (1986). The Continental-Shelf Bottom Boundary Layer. *Annual Review of Fluid Mechanics*, *18*(1), 265-305. doi: 10.1146/annurev.fl.18.010186.001405

Guy, H. P., Simons, D. B., & Richardson, E. V. (1966). *Summary of Alluvial Channel Data from Flume Experiments, 1956-61.* US Government Printing Office.

Hairsine, P. B., & Rose, C. W. (1992). Modeling Water Erosion Due to Overland Flow Using Physical Principles: 1. Sheet Flow. *Water Resources Research*, *28*(1), 237-243. doi: 10.1029/91WR02380

Hjulström, F. (1935). Studies of the Morphological Activity of Rivers as Illustrated by the River Fyris: Bulletin of the Geological Institute of Uppsala, v. 25.

Houssais, M., & Lajeunesse, E. (2012). Bedload Transport of A Bimodal Sediment Bed. *Journal of Geophysical Research: Earth Surface*, *117*(F4). doi: 10.1029/2012JF002490

Jain, S. C. (1992). Note on Lag in Bedload Discharge. *Journal of Hydraulic Engineering*, *118*(6), 904-917. doi: 10.1061/(ASCE)0733-9429(1992)118:6(904)

Kleinhans, M. G., & van Rijn, L. C. (2002). Stochastic Prediction of Sediment Transport in Sand-Gravel Bed Rivers. *Journal of Hydraulic Engineering*, *128*(4), 412-425. doi: 10.1061/(ASCE)0733-9429(2002)128:4(412)

Kooi, H., & Beaumont, C. (1994). Escarpment Evolution on High-Elevation Rifted Margins: Insights Derived from A Surface Processes Model that Combines Diffusion, Advection, and Reaction. *Journal of Geophysical Research: Solid Earth*, *99*(B6), 12191-12209. doi: 10.1029/94JB00047

Krone, R. (1962). Flume Studies of the Transport of Sediment in Estuarial Shoaling Processes, Hydraulic Engineering Laboratory and Sanitary Engineering Research Laboratory, University of California, Berkeley, CA, USA.

Lajeunesse, E., Malverti, L., & Charru, F. (2010). Bed Load Transport in Turbulent Flow at the Grain Scale: Experiments and Modeling. *Journal of Geophysical Research:*

Earth Surface, *115*(F4). doi: 10.1029/2009JF001628

Larsen, I. J., & Lamb, M. P. (2016). Progressive Incision of the Channeled Scablands by Outburst Floods. *Nature*, *538*(7624), 229–232. doi: 10.1038/nature19817

Le Minor, M., Davy, P., Howarth, J., & Lague, D. (2022, October). *Supporting data tables and Python scripts for the paper: "Multi Grain-Size Total Sediment Load Model Based on the Disequilibrium Length".* Zenodo. doi: 10.5281/zenodo.7221833

Liu, M. X., Pelosi, A., & Guala, M. (2019). A Statistical Description of Particle Motion and Rest Regimes in Open-Channel Flows Under Low Bedload Transport. *Journal of Geophysical Research: Earth Surface*, *124*(11), 2666-2688. doi: 10.1029/2019JF005140

Martin, R. L., Jerolmack, D. J., & Schumer, R. (2012). The Physical Basis for Anomalous Diffusion in Bed Load Transport. *Journal of Geophysical Research: Earth Surface*, *117*(F1). doi: 10.1029/2011JF002075

Meyer-Peter, E., & Müller, R. (1948). Formulas for Bed-Load Transport. In *Proc. 2nd IAHR Congress, pp. 39-64.*

Naqshband, S., McElroy, B., & Mahon, R. C. (2017). Validating a Universal Model of Particle Transport Lengths with Laboratory Measurements of Suspended Grain Motions. *Water Resources Research*, *53*(5), 4106-4123. doi: 10.1002/2016WR020024

Nielsen, P. (1992). *Coastal Bottom Boundary Layers and Sediment Transport (Chapter 3)* (Vol. 4). World Scientific.

Parker, G., Klingeman, P. C., & McLean, D. G. (1982). Bedload and Size Distribution in Paved Gravel-Bed Streams. *Journal of the Hydraulics Division*, *108*(4), 544-571. doi: 10.1061/JYCEAJ.0005854

Parker, G., & Toro-Escobar, C. M. (2002). Equal Mobility of Gravel in Streams: The Remains of the Day. *Water Resources Research*, *38*(11), 46-1-46-8. doi: 10.1029/2001WR000669

Partheniades, E. (1965). Erosion and Deposition of Cohesive Soils. *Journal of the Hydraulics Division*, *91*(1), 105-139. doi: 10.1061/JYCEAJ.0001165

Recking, A. (2009). Theoretical Development on the Effects of Changing Flow Hydraulics on Incipient Bed Load Motion. *Water Resources Research*, *45*(4). doi: 10.1029/2008WR006826

Ribberink, J. S. (1998). Bed-load Transport for Steady Flows and Unsteady Oscillatory Flows. *Coastal Engineering*, *34*(1), 59-82. doi: 10.1016/S0378-3839(98)00013-1

Rose, C. P., & Thorne, P. D. (2001). Measurements of Suspended Sediment Trans-

port Parameters in a Tidal Estuary. *Continental Shelf Research*, *21*(15), 1551-1575. (Nearshore and Coastal Oceanography) doi: 10.1016/S0278-4343(00)00087-X

Rouse, H. (1937). Modern Conceptions of the Mechanics of Fluid Turbulence. *Transactions of the American Society of Civil Engineers*, *102*(1), 463-505. doi: 10.1061/TACEAT.0004872

Santini, W., Camenen, B., Le Coz, J., Vauchel, P., Guyot, J.-L., Lavado, W., ... Martinez, J.-M. (2019). An Index Concentration Method for Suspended Load Monitoring in Large Rivers of the Amazonian Foreland. *Earth Surface Dynamics*, *7*(2), 515–536. doi: 10.5194/esurf-7-515-2019

Shields, A. (1936). Anwendung der Aenlichkeitsmechanik und der Turbulenzforschung auf die Geschiebebewegung. Mitteilungen der Preussischen Versuchsanstalt fur Wasserbau and Schiffbau, Berlin, Germany.

Smart, G., & Jaeggi, M. (1983). Sediment Transport on Steep Slopes, Mitt. 64. *Versuch. flit Wasserbau, Hydrologie und Glaziologie, ETH, Zurich*.

Soulsby, R., & Whitehouse, R. (1997). Threshold of Sediment Motion in Coastal Environments. In *Pacific Coasts and Ports 97: Proceedings of the 13th Australasian Coastal and Ocean Engineering Conference and the 6th Australasian Port and Harbour Conference; Volume 1. Christchurch, N.Z.: Centre for Advanced Engineering, University of Canterbury, 1997: [145]-[150].*

Turowski, J. M., Rickenmann, D., & Dadson, S. J. (2010). The Partitioning of the Total Sediment Load of a River into Suspended Load and Bedload: a Review of Empirical Data. *Sedimentology*, *57*(4), 1126-1146. doi: 10.1111/j.1365-3091.2009.01140.x

Vanoni, V. A., & Brooks, N. H. (1957). *Laboratory studies of the roughness and suspended load of alluvial streams* (No. 11). US Army Engineer Division, Missouri River.

van Rijn, L. C. (1982). Equivalent Roughness of Alluvial Bed. *Journal of the Hydraulics Division*, *108*(10), 1215-1218. doi: 10.1061/JYCEAJ.0005917

van Rijn, L. C. (1984a). Sediment Transport, Part i: Bed Load Transport. *Journal of Hydraulic Engineering*, *110*(10), 1431-1456. doi: 10.1061/(ASCE)0733-9429(1984)110:10(1431)

van Rijn, L. C. (1984b). Sediment Transport, Part ii: Suspended Load Transport. *Journal of Hydraulic Engineering*, *110*(11), 1613-1641. doi: 10.1061/(ASCE)0733-9429(1984)110:11(1613)

van Rijn, L. C. (1984c). Sediment Transport, Part iii: Bed Forms and Alluvial Roughness.

Journal of Hydraulic Engineering, *110*(12), 1733-1754. doi: 10.1061/(ASCE)0733-9429(1984)110:12(1733)

Wilcock, P. R. (1993). Critical Shear Stress of Natural Sediments. *Journal of Hydraulic Engineering*, *119*(4), 491-505. doi: 10.1061/(ASCE)0733-9429(1993)119:4(491)

Wilcock, P. R., & Crowe, J. C. (2003). Surface-Based Transport Model for Mixed-Size Sediment. *Journal of Hydraulic Engineering*, *129*(2), 120-128. doi: 10.1061/%28ASCE%290733-9429%282003%29129%3A2%28120%29

Wilcock, P. R., Kenworthy, S. T., & Crowe, J. C. (2001). Experimental Study of the Transport of Mixed Sand and Gravel. *Water Resources Research*, *37*(12), 3349-3358. doi: 10.1029/2001WR000683

Wong, M., & Parker, G. (2006). Reanalysis and Correction of Bed-Load Relation of Meyer-Peter and Müller Using Their Own Database. *Journal of Hydraulic Engineering*, *132*(11), 1159-1168. doi: 10.1061/(ASCE)0733-9429(2006)132:11(1159)

Yalin, M. S. (1972). *Mechanics of Sediment Transport, Pergamon Press, New York, NY.*